https://doi.org/10.5194/angeo-2024-16
Preprint. Discussion started: 19 September 2024

Annales Geophysicae Discussions
Open Access
EGU

First Report on Coseismic Ionospheric Disturbances Following the Deep-Focus Earthquake (Mw 6.6) in Tarauacá, Acre, Brazil: Ground Uplift and TEC Analysis

Oluwasegun M. Adebayo[1], Esfhan A. Kherani[1], Alexandre A. Pimenta[1]

[1]Heliophysics, Planetary Science and Aeronomy Division, National Institute for Space Research (INPE), São José dos Campos 12227-010, Brazil

Correspondence to: Oluwasegun M. Adebayo (oluwasegun.adebayo@inpe.br)

Abstract. On January 20, 2024, a deep-focus earthquake of magnitude 6.6 struck near Tarauacá, Brazil, at a depth of 607.0 km. While no surface damage was reported, this event marked a significant seismic occurrence in a region known for deep earthquakes associated with the subducted Nazca Plate. Using Global Navigation Satellite System (GNSS) Total Electron Content (TEC) data from the Brazilian Network for Continuous Monitoring of GNSS Systems (RBMC) and seismic data from the IRIS network, we analyzed the earthquake's impact on both ground surface (in form of uplift) and ionosphere (in form of disturbances). The results show clear ionoquakes characterized by distinct "*N*-type" wave patterns in TEC data, originating from infrasonic-acoustic waves launched from the earthquake's crustal displacement. On avereage, the ionoquakes arrived in the ionosphere 8.3 minutes from the mainshock onset and traveled with the net propagation speed of 550 m/s to 743 m/s. This is the first report on coseismic ionospheric disturbances, or ionoquakes, following an earthquake in the Brazilian sector. The spectral analysis shows a maximum TEC amplitude in the frequency range 14 mHz – 16 mHz which suggest that the ionoquakes are signatures of high-frequency infrasonic-acoustic waves dynamics.

Keywords: coseismic ionospheric disturbances (CIDs), deep-focus earthquake, LAI coupling, GNSS receivers, Total Electron Content (TEC)

1 Introduction

On January 20, 2024, a deep-focus earthquake struck near Tarauacá, Acre, Brazil. The United States Geological Survey (USGS) reported the earthquake with a magnitude (Mw) of 6.6 at 21:31:05 UT, located at coordinates 7.288°S latitude and 71.464°W longitude, with a focal depth of 607.0 km, approximately 123 km northwest of Tarauacá. This event occurred in a region known for deep

https://doi.org/10.5194/angeo-2024-16
Preprint. Discussion started: 19 September 2024


Annales Geophysicae Discussions

earthquakes associated with deformation within the subducted Nazca Plate (Cahill and Isacks, 1992; Hasegawa and Sacks, 1981). While the earthquake was felt at the epicenter, no significant damage was recorded. The substantial depth of the earthquake likely mitigated its impact in absolute terms, despite its considerable magnitude. Brazil experiences relatively few earthquakes due to its central location atop the South American tectonic plate, away from its more seismically active edges (Castaños and Lomnitz, 2012; Takeya, 1992). However, two notable earthquakes occurred in January 2024, on the 20th and 28th. Historically, most moderate to large earthquakes (> Mw 6.0) reported in Brazil have occurred at depths exceeding 500 km, with exceptions such as the 1955 event in Mato Grosso at a shallower depth of 15 km (USGS Earthquake Hazards Program).

When earthquakes occur, the majority of the seismic energy propagates through the Earth's interior as body waves and surface waves. Simultaneously, the sudden release of energy from ground displacement generates acoustic and gravity waves in the atmosphere, which can create shock waves as they propagate upwards, influenced by changes in neutral density (Kherani et al., 2009; Lognonné and Garcia, 2006; Hines, 1960). This energy transfer typically manifests as infrasonic acoustic waves (Sunil et al., 2022; Hamama et al., 2021; Chum et al., 2016; Lognonné et al., 1998), causing oscillations in the neutral atmosphere and perturbing ion and electron densities in the ionospheric plasma (Kherani et al., 2012;2009). These disturbances, known as Coseismic Ionospheric Disturbances (CIDs or ionoquakes), are well-documented phenomena (Sanchez et al., 2023; Maletckii et al., 2023; Sunil et al., 2022; Kherani et al., 2016, 2012, 2009; Astafyeva and Shults, 2019; Davies and Baker, 1965). They typically induce distinct variations in ionospheric parameters such as electron density (or Total Electron Content, TEC) (Maletckii et al., 2023; Rolland et al., 2011; Astafyeva et al., 2009), electron temperature (Sharma et al., 2006), ionic composition (Zhang et al., 2009), and magnetic field (Santis et al., 2019; Kherani et al., 2009). In GPS-TEC time series, these earthquake-related signals often appear as an “N” wave or an inverted “N” wave (Maletckii et al., 2023; Astafyeva et al., 2013; Astafyeva and Heki, 2009).

Based on literature, there have been no documented cases of ionoquakes associated with earthquakes in the Brazilian region, possibly due to the majority of earthquakes occurring at depths greater than 200 km, which makes their detection in the ionosphere challenging. Sunil et al. (2021) examined various

https://doi.org/10.5194/angeo-2024-16
Preprint. Discussion started: 19 September 2024

tectonic factors influencing ionoquake amplitudes, highlighting focal depth as a significant parameter. They noted that shallow earthquakes produce pronounced surface displacements localized to smaller areas, whereas deep earthquakes result in smaller surface displacements spread over broader regions (Sunil et al., 2021). However, they did not establish a precise depth threshold for generating detectable ionoquakes.

Perevalova et al. (2014) investigated earthquakes across magnitudes ranging from 4.1 to 8.8 and identified a threshold magnitude of 6.5 for Ionospheric Total Electron Content (TEC) responses, implying that ionoquakes associated with earthquakes below this magnitude are likely to be undetectable. Nevertheless, Sanchez et al. (2022) documented clear ionoquakes following a 6.4 magnitude earthquake in Ridgecrest, California, USA, indicating cases where ionospheric responses were observed below the 6.5 threshold. Similarly, Maletckii et al. (2023) analyzed ionoquakes following the February 6, 2023 earthquake, observing ionospheric responses to aftershocks of magnitudes 6.0 and 5.6. Therefore, the ionospheric response to seismic origin seems to be vastly controlled by several factors which are still under investigations.

In this study, we present the first documented coseismic ionospheric disturbances following the 6.6 magnitude deep-focus earthquake in the Brazilian sector. Using Global Navigation Satellite System (GNSS) Total Electron Content (TEC) data obtained from receivers in the Brazilian Network for Continuous Monitoring of GNSS Systems (RBMC) and seismometer data from the IRIS network, we analyzed the earthquake using the ground uplift and TEC data. Our investigation focused on data from the nearest monitoring stations to minimize noise. The structure of this paper is as follows: Section 2 outlines our data and methods for analysis, Section 3 presents the results including ground uplift from the NNA seismometer and dTEC from Brazilian GNSS receivers, along with travel-time diagrams (TTD) and spectrograms showing the comparative analysis of both ground uplift and TEC disturbances dynamical spectrum. Section 4 discusses these findings, and Section 5 provides a summary and conclusion.

https://doi.org/10.5194/angeo-2024-16
Preprint. Discussion started: 19 September 2024

Annales Geophysicae Discussions

2.0 Data and Methods

In this study, we used seismic and TEC data to analyze ground uplift and associated ionospheric disturbances. Ground uplift data were obtained from the nearest seismometer (NNA/II network) via the IRIS network, located 788 km from the epicenter in Nana, Peru. We processed the vertical component of the seismogram using the ObsPy Python library (Krischer et al., 2015; Sanchez et al., 2023, 2022). Additionally, we considered multiple GNSS receivers positioned near the earthquake epicenter within the permanent ground-based RBMC network. These receivers recorded phase and range characteristics of GNSS satellite radio signals at two distinct frequencies. The data, formatted in RINEX, were sampled at 15-second intervals, and we used the "tec-suite" software to derive slight Total Electron Content (sTEC). According to Hofmann-Wellenhof (2007), TEC is calculated using the expression below:

$$TEC = \frac{1}{40.308}\frac{f_1^2 f_2^2}{f_1^2 - f_2^2}(L_1\lambda_1 - L_2\lambda_2 + const + nL),$$

In this context, $f_1 = 1575.42MHz$ and $f_2 = 1227.60MHz$ represent carrier-wave frequencies, $\lambda_1 = \frac{c}{f_1}$ and $\lambda_2 = \frac{c}{f_2}$ denote the corresponding wavelengths in meters. Here, c represents the speed of light, L_1 and L_2 stand for carrier phases, $const$ represents the unknown initial phase ambiguity, and nL signifies the error in determining the phase path. Total Electron Content (TEC) is measured in TEC units (TECU), where 1 TECU corresponds to 10^{16} electrons per square meter. The vertical Total Electron Content (vTEC) is obtained from *sTEC* through the application of the conversion equation below (Klobuchar, 1987):

$$vTEC = sTEC \times \cos\left(arcsin\left(\frac{r_e}{r_e + H_{ion}}cos\theta_{el}\right)\right)$$

r_e represents the radius of the Earth, H_{ion} signifies the altitude of the ionospheric thin layer (250 km), and θ_{el} is the elevation angle of the satellite. The data analysis steps go as thus: all data from "tec-suite" are inputted into the analysis code, selecting receivers with a 15-second sampling interval, ensuring satellite elevation angles exceed 20°, calculated the $vTEC$, and calculated the dTEC using convolution

https://doi.org/10.5194/angeo-2024-16
Preprint. Discussion started: 19 September 2024


Annales Geophysicae Discussions

method at 60 seconds window. A running mean average is applied in the frequency range of 1.5-33 mHz to detrend TEC data from background variations due to tidal and low-frequency gravity wave dynamics. The residual TEC disturbance, dTEC, is derived from detrended TEC data by applying a running mean average in the 3-20 mHz frequency range, focusing on TEC disturbances in infrasonic-acoustic frequencies (Hamama et al., 2021; Chum et al., 2016). This method, similar to approaches used by Sanchez et al. (2022), Zhai et al. (2021), and Afraimovich et al. (2001), has demonstrated efficacy in detecting localized transient events such as ionoquakes.

2.1 Wavelet/Time-Frequency Analysis

Wavelet analysis is a technique used to examine the time-frequency characteristics of a signal, and it is particularly useful for analyzing non-stationary signals (Torrence and Compo, 1998). By decomposing the Total Electron Content (TEC) data into different frequency components over time, we can observe how these components vary and detect specific patterns related to ionospheric disturbances.

We first applied the Fast-Fourier Transform (FFT) to the dTEC data using the Python SciPy module. FFT is a frequency-domain technique that decomposes the signal into its constituent frequencies but does not provide time-localized information. Following FFT, we computed the power density of the signal at different frequencies. This quantifies the intensity or strength of each frequency component. We used the "*find_peaks*" function from the SciPy module to identify peaks in the power density spectrum. This step helps in determining significant frequencies and their corresponding periods. The "wavelet" code performs time-frequency analysis using a simple boxcar (moving average) filter and returns two main parameters: (1) the power density, and (2) the decomposition elements.

We calculated the frequency associated with the power density using the following formula:

$$\text{frequency (mHz)} = \frac{10^3}{\text{power\_density} \times 3600}$$

https://doi.org/10.5194/angeo-2024-16
Preprint. Discussion started: 19 September 2024

Here, the scaling factor 10^3 adjusts the units to milliseconds (ms), and the multiplication by 3600 converts from hours to seconds, reflecting the time span corresponding to each frequency component.

Figure 1 illustrates the earthquake epicentre marked with a red star, GNSS receiver positions denoted by blue dots, the seismometer location indicated by a green triangle, and ionospheric piercing points (IPP) showing satellite trajectories in pink lines, one hour before and two hours after the earthquake. The position of the satellites at the time of the earthquake is shown as the cyan diamonds along the IPP trajectories for both PRN 09 and PRN 17. Our analysis focuses exclusively on GNSS receivers that recorded ionoquakes and located in the closest proximity to the epicentre, alongside the nearest seismometer. Moreover, the sparse distribution of GNSS receivers in the State of Acre, where the earthquake occurred, necessitates concentrating on the four receivers depicted in Figure 2 (blue dots) to minimize data noise.

https://doi.org/10.5194/angeo-2024-16
Preprint. Discussion started: 19 September 2024

Figure 1: Red star indicates the epicentre of the (Mw 6.6) earthquake on January 20th 2024, blue dots indicate the position of the GNSS receivers that recorded ionoquakes, blue 'x' show the position of the other receivers that are either without data or did not record ionoquakes, magenta lines indicate the IPP trajectories in 1 hour before the earthquake and 2 hours after the earthquake, cyan diamonds indicate the position of the satellites when the earthquake occurred, and the green triangle indicates the position of the closest seismometer to the epicentre. Magnetic equator is shown as the dashed black line running from west to east.

3 Results

Two PRNs, 9 and 17, observed coseismic ionospheric disturbances following the 6.6 Tarauacá, Brazil earthquake on the 20th January 2024 at 21:31:05 UT. The ground uplift, sTEC and dTEC sigantures are shown in Figure 2. Figure 2(a) shows the slight TEC, sTEC for two selected receivers as observed by PRN 09 and PRN 17 (a1 and a2). dTEC obtained from the sTEC data is shown in (b1) and (b2). These two receivers observe a clear "*N*-type" wave pattern usually attributed to the signature of coseismic ionospheric disturbances associated with earthquake. (c) shows the ground uplift obtained from the

https://doi.org/10.5194/angeo-2024-16
Preprint. Discussion started: 19 September 2024

Nana, Peru seismometer station (NNA/II IRIS Network) and it's the closest to the epicenter. The figure illustrates that ground uplift took off at 21:55 UT and reached a maximum velocity of 1.0 cm/s, approximately 1.8 minutes after the earthquake. This delay could be attributed to the distance between the seismometer and the earthquake epicenter which is 788 km. Furthermore, the observed ground uplift of 1.0 cm/s exceeds the 0.6 cm/s reported for the 6.4 magnitude Ridgecrest earthquake (Sanchez et al., 2022), and is notably larger than the 0.01 cm/s recorded in France following the 1999 Chi-Chi earthquake (Artru et al., 2004). Thus, based on the previous studies, the uplift is substantial.

Analysis of ionospheric space weather conditions at the equatorial region on the day of the event (January 20th 2024) indicated extremely quiet geomagnetic conditions with Dst > -13 nT. January 2024 was generally characterized by very low geomagnetic activity based on Gonzalez et al. (1994) classification, with a minimum Dst value of -27 nT (Source: https://wdc.kugi.kyoto-u.ac.jp/dst_realtime/202401/index.html). Consequently, the influence of forcing above (e.g., geomagnetic storms) on the ionosphere on the day of the earthquake was relatively minimal, favoring forcing below processes such as earthquakes.

https://doi.org/10.5194/angeo-2024-16
Preprint. Discussion started: 19 September 2024

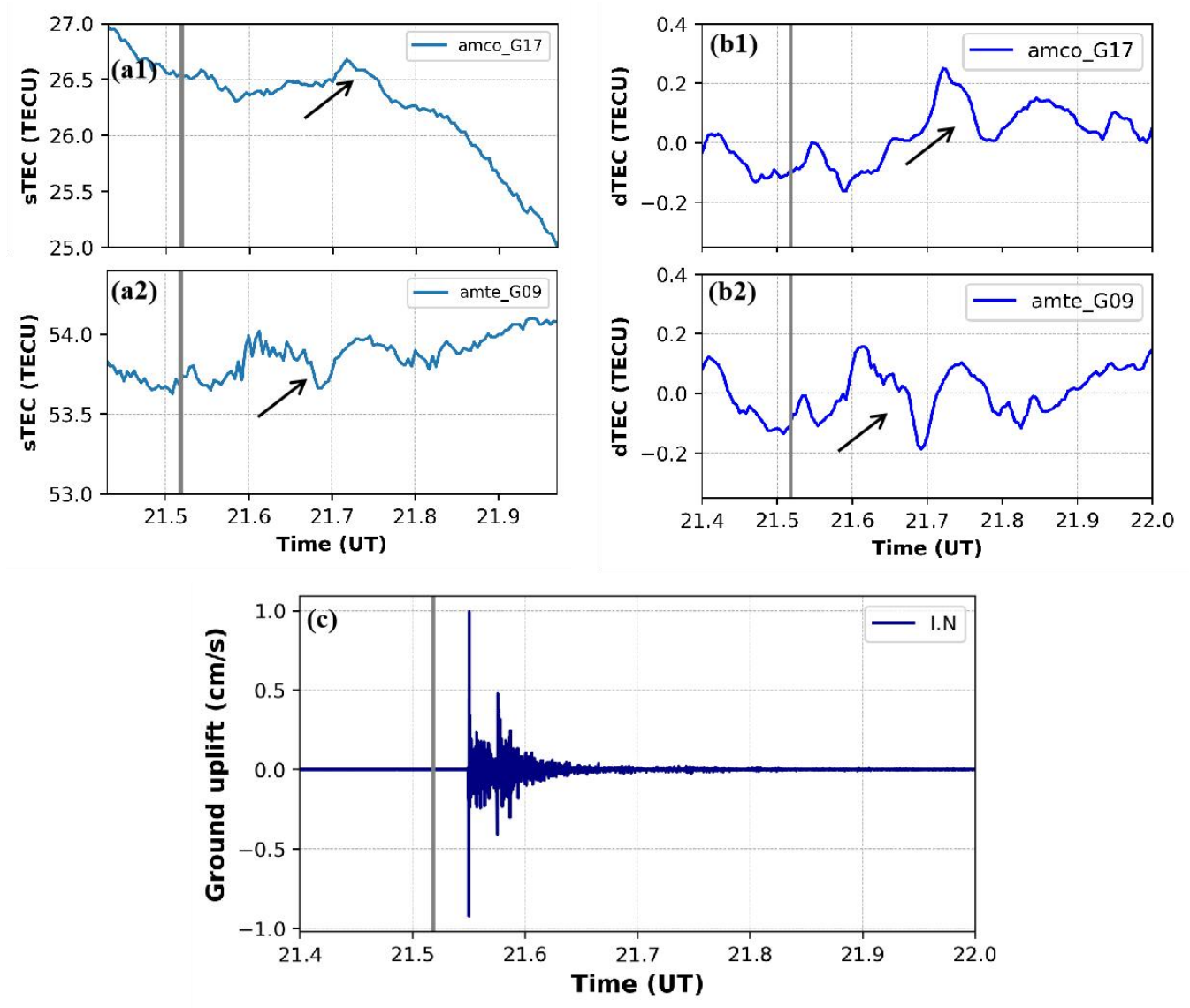

Figure 2: (**a**) shows the slight TEC (sTEC) for two selected receivers as observed by PRN 09 and PRN 17 (**a1** and **a2**). dTEC obtained from the sTEC data is shown in (**b1**) and (**b2**). These two receivers observe a clear "*N*-type" wave pattern usually attributed to the signature of coseismic ionospheric disturbances associated with earthquake. **(c)** shows the ground uplift obtained from the Nana, Peru seismometer station (NNA/II Network) and it's the closest to the epicenter.

https://doi.org/10.5194/angeo-2024-16
Preprint. Discussion started: 19 September 2024

The dTEC derived from the four closest receivers was used to construct a travel-time diagram (TTD), depicting shifts in both time and space, commonly used to correlate amplified waveforms post-earthquake with fault regions (Maletckii et al., 2023; Sanchez et al., 2022; Zhai et al., 2021; Kherani et al., 2012). Figure 3 shows the TTD for the earthquake day (left panel) and the previous day (right panel) across several ionospheric Piercing Point (IPP) trajectories for PRN 09 and PRN 17. Each trajectory represents a five-point running mean, enhancing visibility of the "*N*-type" wave pattern typical of ionoquakes of the seismic origin (Maletckii et al., 2023; Sunil et al., 2021; Astafyeva et al., 2019).

On the EQ Day, a distinct "*N*-type" wave pattern appear around 330 seconds after the mainshock, particularly evident at receivers "amte_G09" and "amco_G17". The receiver "AMTE" recorded the highest absolute TEC amplitude of 0.20 TECU, probably due to its proximity to the epicenter at a similar latitude. In addition, "AMTE" detected ionoquakes earlier, starting at 330 seconds (5.5 minutes), whereas "AMCO", the farthest from the epicenter, observed them later at 740 seconds (12.33 minutes). Thus, ionoquakes were observed by receivers within a timeframe of 5.5 to 12.33 minutes post-mainshock, consistent with arrival times reported by Li et al. (2024), Maletkii et al. (2023), Ruan et al. (2023), Sanchez et al. (2023), and Heki (2021).

The delay between the mainshock and the onset of ionospheric disturbances is attributed to the propagation of direct acoustic waves, launched from the crustal displacement, from the ground to ionospheric altitudes (Maruyama et al., 2012; Tanaka et al., 1984). Using the TTD in latitude and longitude, we estimated the net propagation speeds of ionoquakes to range from 550 m/s to 743 m/s. Such velocities below 1.0 km/s are characteristic of acoustic or gravity waves (Maruyama et al., 2012). Thus, the ionoquakes travel with the thermospheric sound speed (see Figure S1 - sound speed profile) and are signatures of direct acoustic waves launched from the epicenter (Heki, 2021). Zhai et al. (2021) reported propagation speeds of ionospheric disturbances following the Tohoku earthquake ranging from 666 m/s to 724 m/s, attributing them to infrasonic-acoustic waves, while Sanchez et al. (2023) documented speeds of 750 m/s following the Illapel and Iquique earthquakes. Thus, our findings agree with previous studies (Vashisth et al., 2024; Sanchez et al., 2023; Ruan et al., 2023; Astafyeva and Shultz, 2019; Rolland et al., 2011a).

https://doi.org/10.5194/angeo-2024-16
Preprint. Discussion started: 19 September 2024

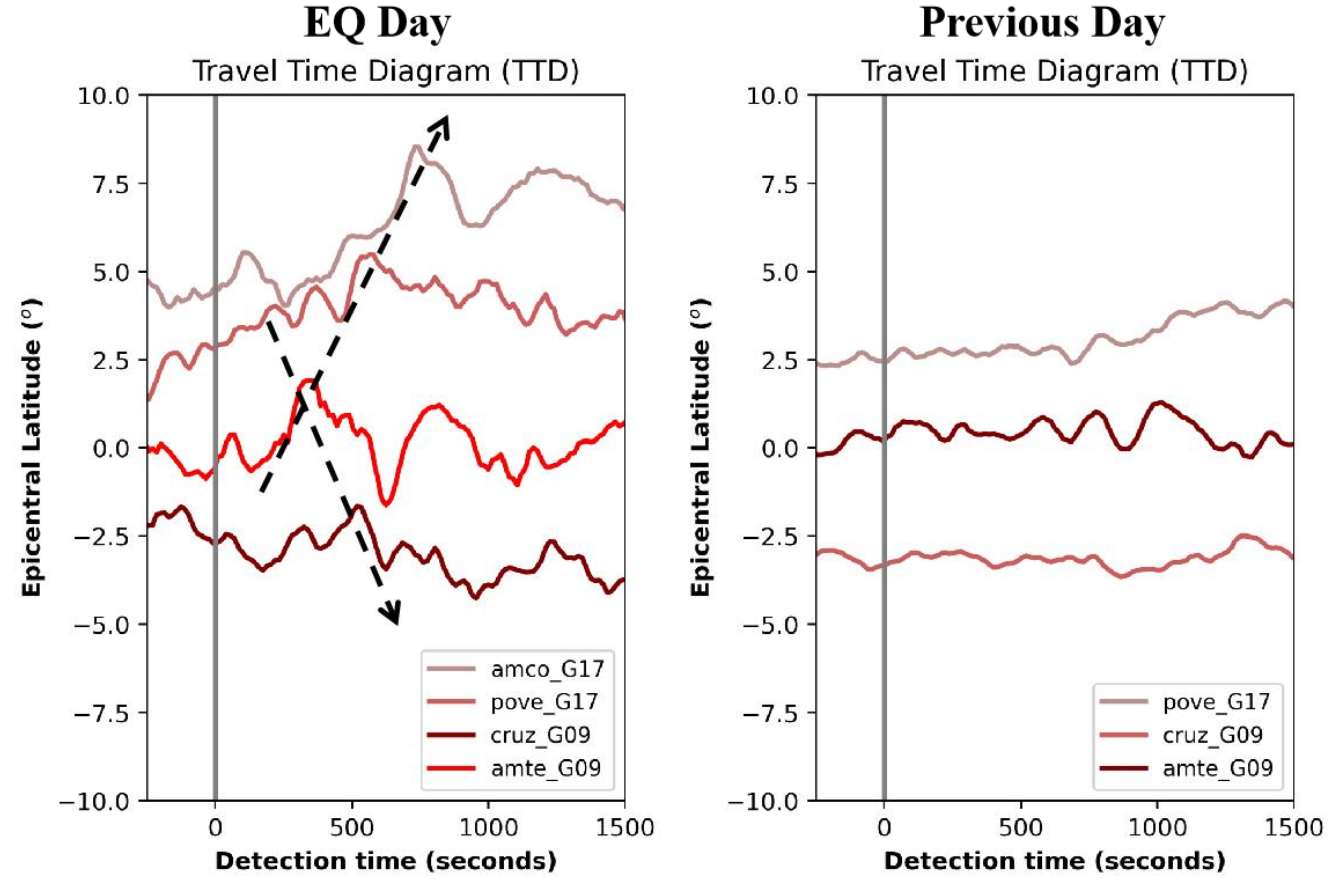

Figure 3: Travel-Time-Diagram (TTD) as a function of time and the epicentral latitude for the day of earthquake (left panel) and the previous day (right panel) for selected GNSS receivers as observed by PRN 09 and PRN 17. Dashed black arrows show shift in both space (epicentrial latitude) and time (detection time) with a clear acoustic structure. It further shows that the TEC disturbances radially propagate away from the epicenter. Grey thick line indicates the time of earthquake. Detection time (seconds) $= (\text{time}_{\text{rec}}\ (\text{UT}) - \text{time}_{\text{epi}}\ (\text{UT})) \times 3600$ where time_{rec} is the record time and time_{epi} is the time of earthquake (21:31:05 UT). Epicentral latitude (°) $= \text{lat}_{\text{ipp}}\ (°) - \text{lat}_{\text{epi}}\ (°)$ where lat_{ipp} is obtained from the IPP trajectories and lat_{epi} is the latitude of the epicentre.

https://doi.org/10.5194/angeo-2024-16
Preprint. Discussion started: 19 September 2024


Annales Geophysicae Discussions

With the target to understand the mechanisms behind the ionoquakes associated with this earthquake, we resampled the ground uplift data to a 15-second interval to match the TEC sampling interval, shown in Figure 4 (upper panel). Additionally, we computed the average dTEC using all the four receivers shown in Figure 3, presented in Figure 4 (lower panel). Apparently, an "*N*-type" wave pattern typically linked to TEC disturbances originating from seismic events still appear, reaffirming the findings observed in Figures 2 and 3 as distinct signatures of this earthquake in the ionosphere – ionoquakes.

According to Artru et al. (2001), ionospheric perturbations typically manifest in the frequency domain ranging from 1 mHz to 50 mHz. The spectrum of ionoquakes depends on atmospheric viscosity, ground uplift amplitude, and the nonlinear dynamics of lower atmosphere-ionosphere coupling (Chum et al., 2016). Consequently, we subjected the data in Figure 4 to wavelet spectral analysis, presenting the results in Figure 5 as spectrograms (dynamical spectral): ground uplift on the left panel and TEC on the right panel. The red lines in the TEC spectrograms represent average TEC data from the previous day, where no evident "N-type" wave pattern is identifiable.

The TEC spectrograms reveal two principal bands of frequency perturbations: 8 mHz to 10.5 mHz and 14 mHz to 16 mHz, corresponding to low and high-frequency ionoquakes, respectively. Below 10 mHz, which is extensively studied in previous research, ionoquake amplitudes are relatively smaller, with a maximum of 0.013 TECU, compared to higher frequencies above 10 mHz, where the maximum amplitude reaches 0.03 TECU. In addition, the highest amplitudes are concentrated in the 14 mHz to 16 mHz frequency range. Kherani et al. (2012) conducted simulations of TEC disturbances following the Tohoku-Oki tsunami, observing the early arrival of high-frequency components of disturbances within 6-7 minutes, emphasizing the significance of high-frequency components in the ionospheric response to natural hazards. This observation is consistent with the concept that high-frequency disturbances have faster phase velocities, leading to their earlier arrival compared to lower-frequency components. The faster phase velocity of these high-frequency waves means they propagate more quickly through the ionosphere, aligning with the observed earlier arrival times in our data. The spectral characteristics of ionoquakes depicted in Figure 5 resemble findings reported by Chum et al. (2016) in Taiwan during the

https://doi.org/10.5194/angeo-2024-16
Preprint. Discussion started: 19 September 2024

Tohoku-Oki earthquake, highlighting a spectral peak of ionoquakes in the 10-20 mHz range, different from ground uplift peaks at frequencies higher than 20 mHz.

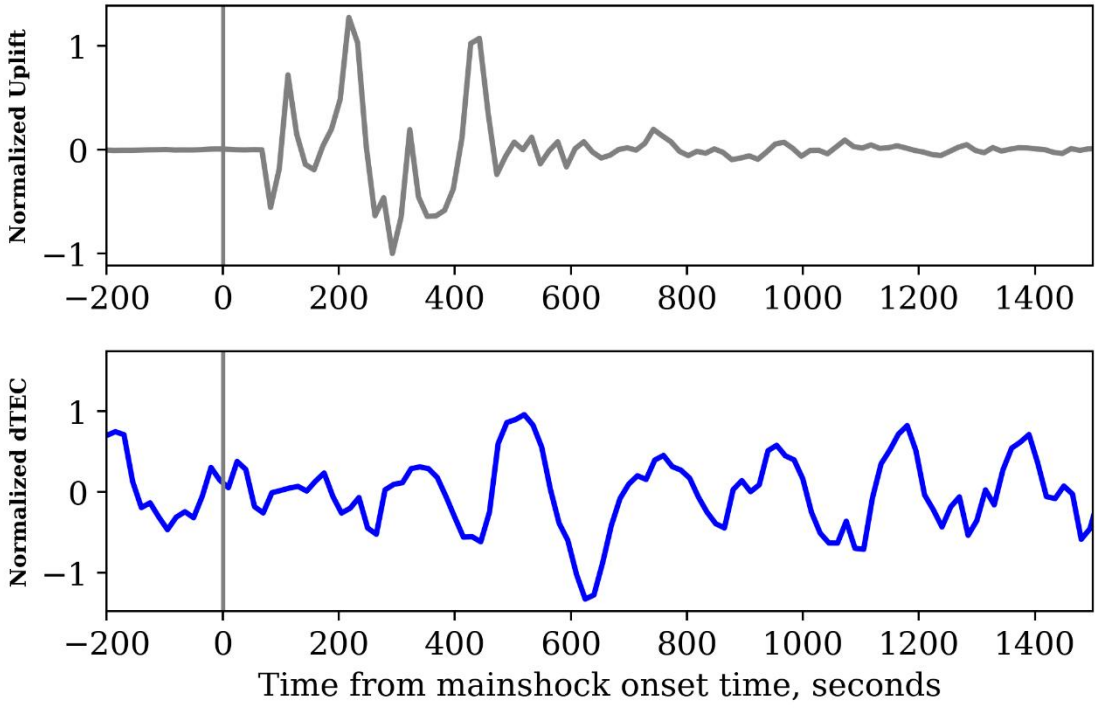

Figure 4: Upper panel shows the resampled (15 seconds) normalized ground uplift and lower panel is the normalized average of the dTEC from the receivers in figure 3.

255

Similarly, the frequency distribution observed in the ground uplift strongly correlates with the TEC spectrograms, suggesting a clear cause-and-effect relationship between ground vibrations and ionospheric TEC disturbances. The ground uplift spectrograms also reveal two prominent frequency bands: 8 mHz to 10.5 mHz and above 14 mHz. The first band aligns closely with frequencies observed
260 in the TEC disturbances, while the peak frequency of ground uplift at 16 mHz coincides with the range of 14 mHz to 16 mHz in the TEC disturbances. A correlation coefficient of +0.918 (p-value < 0.0005) indicates a statistically significant positive correlation between ground uplifts and ionoquakes. This suggests that the ionoquake spectrum results from combined ground uplift effects mediated by

https://doi.org/10.5194/angeo-2024-16
Preprint. Discussion started: 19 September 2024


Annales Geophysicae Discussions

lithosphere-atmosphere-ionosphere coupling, energized by infrasonic-acoustic waves. According to Zettergen and Snively (2015), acoustic waves in the narrow band of 1-4 minutes, corresponding to 4-16 mHz from impulsive sources (like earthquakes), propagate through the viscous thermosphere, generating identifiable TEC disturbances. The dominance of the 4-16 mHz spectral range in Figure 5 implies the role of infrasonic-acoustic wave dynamics in the observed ionoquakes in this study, with high-frequency disturbances arriving earlier probably due to their faster phase velocities.

https://doi.org/10.5194/angeo-2024-16
Preprint. Discussion started: 19 September 2024

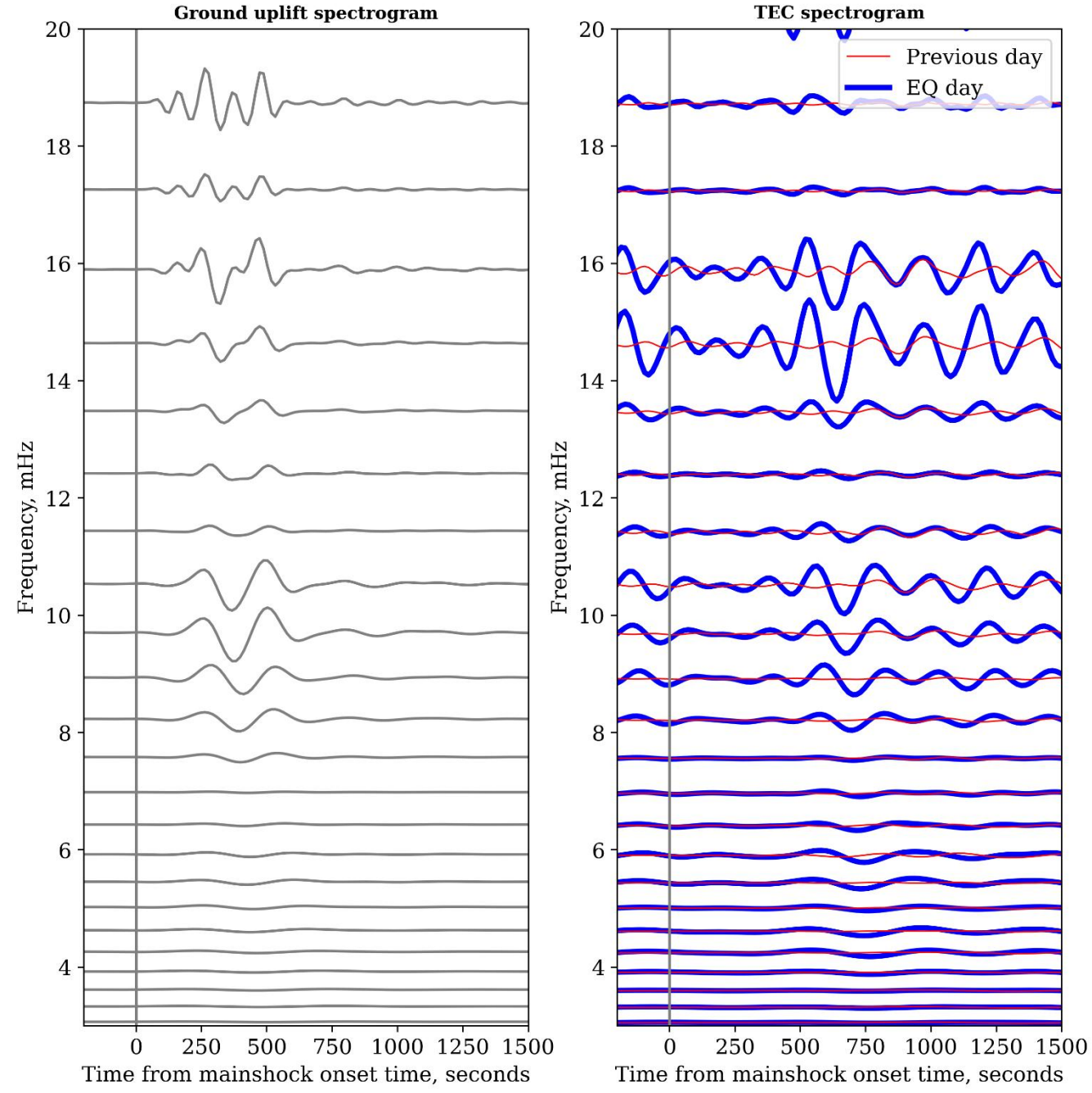

Figure 5: Ground uplift spectrogram (left panel) in the frequency range 3 mHz – 20 mHz. TEC spectrogram for the EQ Day (in blue) and TEC spectrogram for the previous day (in red). Grey vertical line at 0 seconds represents the mainshock onset time.

285

https://doi.org/10.5194/angeo-2024-16
Preprint. Discussion started: 19 September 2024

To study the relationship between ground uplift and TEC disturbances further, we extracted the maximum ground uplift and TEC amplitudes from the spectrograms in Figure 5 for each frequency, as illustrated in Figure 6. Using the Python "find_peaks" function from the Scipy module (Virtanen et al., 2020), we identified the TEC values corresponding to these peaks and plotted them against frequency.

Key findings from Figure 6 include: (1) at frequencies ranging from 3 mHz to 7.5 mHz, the smallest ground uplift corresponds to TEC disturbances below 0.005 TECU; (2) from 8 mHz to 11 mHz, as ground uplift increases monotonically, TEC disturbances also increase (0.015 TECU), peaking at 10.5 mHz in a normal distribution pattern; (3) similarly, frequencies greater than 11 mHz exhibit a monotonic increase in ground uplift, resulting in TEC disturbances with a normal distribution, peaking at 0.03 TECU between 14 mHz and 16 mHz; and (4) overall, maximum ground uplift amplitudes linearly increase with frequency, while TEC disturbances display a negatively skewed distribution across frequencies with peak at 14 mHz – 16 mHz.

These observations emphasize the distinct spectral nature of uplifts and ionoquakes, reflecting their different origins: uplifts from the solid earth and ionoquakes from plasma. This divergence in spectral nature is expected due to their respective physical states of matter.

https://doi.org/10.5194/angeo-2024-16
Preprint. Discussion started: 19 September 2024

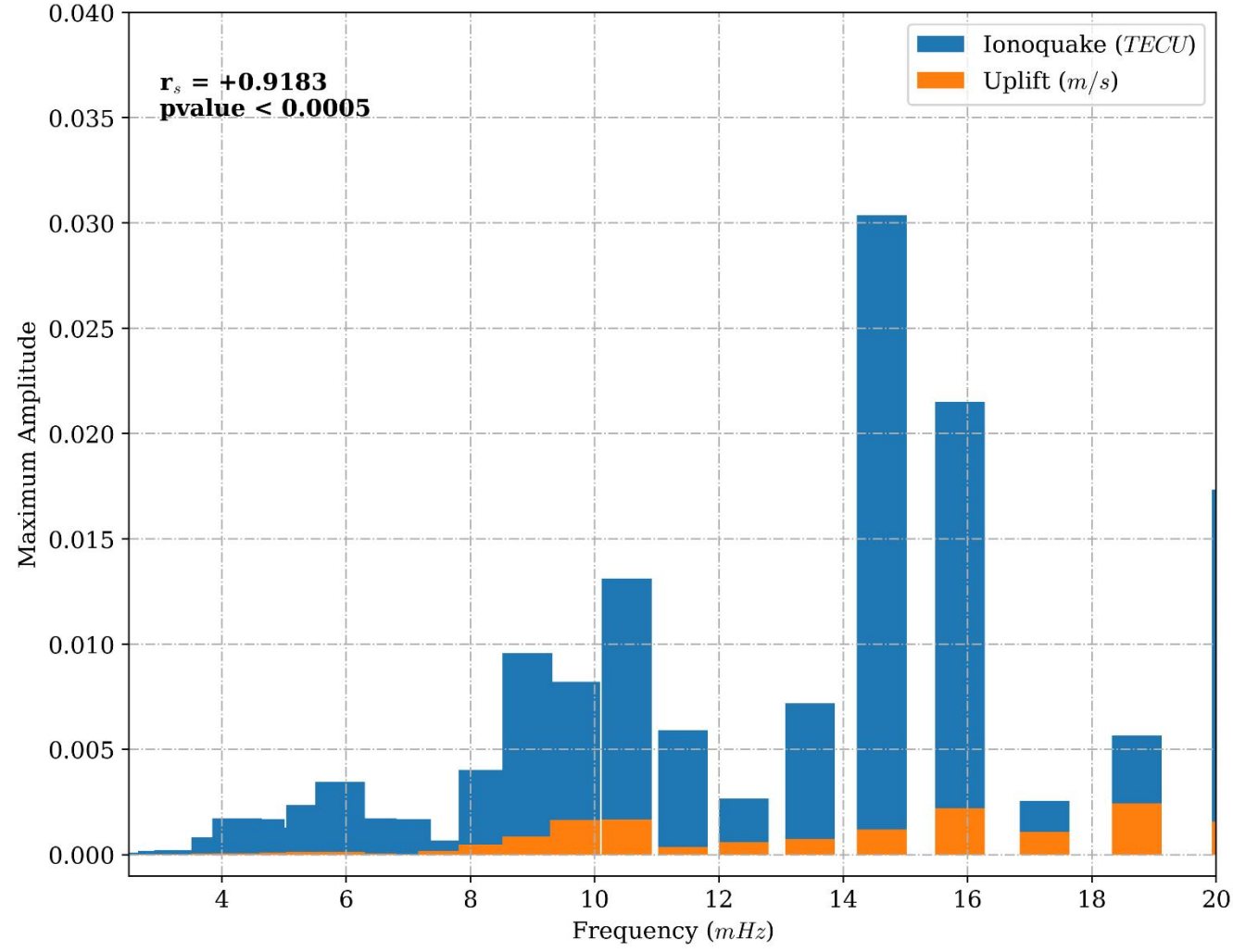

Figure 6: Maximum ground uplift (in orange) and the ionoquake TEC amplitude (in blue) for each frequency.

4 Discussion

Coseismic ionospheric disturbances following medium to large earthquakes have been extensively documented since the seminal work of Davies and Baker (1965), with numerous studies confirming their occurrence (Sanchez et al., 2023; Maletckii et al., 2023; Kherani et al., 2016; Rolland et al., 2011; Astafyeva et al., 2009; Molchanov et al., 1995; Parot and Mogilevsky, 1989). Reports of ionoquakes

https://doi.org/10.5194/angeo-2024-16
Preprint. Discussion started: 19 September 2024

associated with earthquakes of magnitude 6.6 have been reported as well (Cahyadi and Heki, 2015; Perevalova et al., 2014; Astafyeva et al., 2013), but none previously recorded at a focal depth as deep as 600 km, which typically would be expected to produce no identifiable TEC disturbances. Thus, this study is the first to report ionoquakes associated with deep-focus earthquake.

Three (3) factors appear to have favored the detectability of these ionoquakes in this event:

1. The satellites geometry with respect to the GNSS receivers;
2. The local time of the earthquake occurrence (16:00 local time), and
3. Favorable ionospheric background conditions.

Several investigators have identified various factors that influence the ionospheric response to seismic signals. These include earthquake magnitude (Astafyeva and Heki, 2009), focal depth (Sunil et al., 2021), focal mechanism (Cahyadi and Heki, 2015), surface deformation (Sunil et al., 2021), and rupture propagation direction (Li et al., 2024; Sunil et al., 2017; Rolland et al., 2013). The detectability of ionoquakes in TEC data is strongly controlled by the satellites geometry. According to Heki et al. (2006), the angle between the wave front and the line of sight influences the amplitude of visible ionoquakes. This amplitude increases when the wave front and the line of sight are aligned at ionospheric altitudes (Heki et al., 2006). From Figure 7 which shows the elevation angles of the satellite with time and the receivers distance to the epicentre, we can infer that the the decrease in the satellite's elevation angle (for G09 and G17) likely increase the path length through the ionosphere, which could enhance the detectability of the ionoquakes. This is because a longer path through the ionosphere allows for a more pronounced effect of the disturbances on the GPS signal, improving the chances of observing and analyzing these disturbances. Li et al. (2024), among all the satellites that observed the ionoquakes in their work, only the satellite with the lowest elevation angle (40º) observed the clearest '*N*-type' wave. The trajectory is similar to the 'amte_G09' and 'amco_G17' which observed a clear '*N*-type' wave in the ionosphere following the earthquake.

https://doi.org/10.5194/angeo-2024-16
Preprint. Discussion started: 19 September 2024

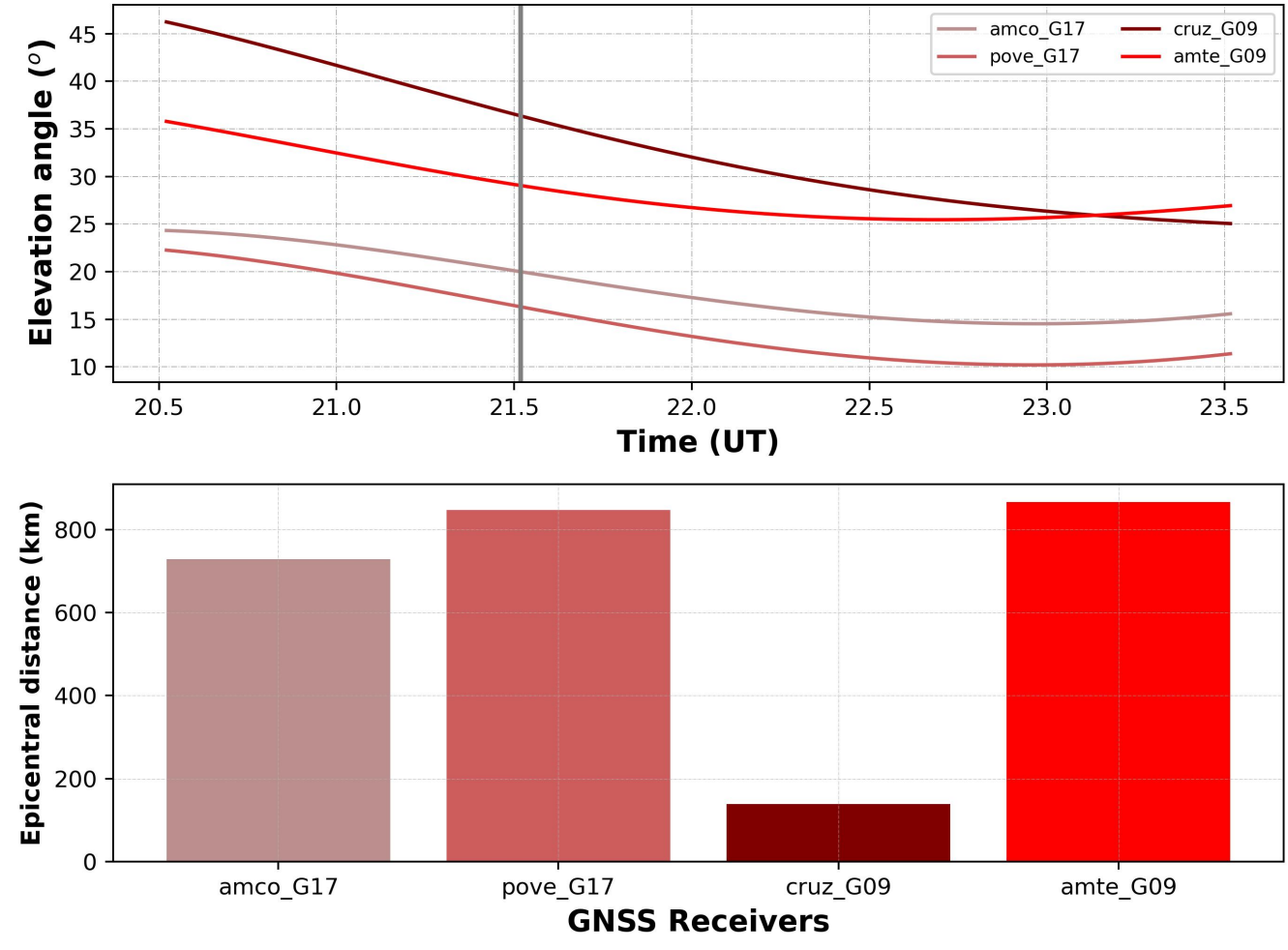

345 Figure 7: Upper panel - elevation angle (°) of the satellites over time (UT). Lower panel - epicentral distance (km) for each GNSS receiver. 'cruz_G09,' the closest receiver, shows a relatively smaller amplitude, likely due to the ionoquakes traveling to the east of the epicenter.

Sunil et al. (2022) analyzed the impact of ionospheric background electron density and geomagnetic
350 field strength on the detection of ionoquakes, noting their significant influence on the orientation and amplitude of Total Electron Content (TEC) disturbances. Additionally, Zettergen and Snively (2019) highlighted the geomagnetic latitude dependency of coseismic ionospheric disturbances, with

https://doi.org/10.5194/angeo-2024-16
Preprint. Discussion started: 19 September 2024

disturbances being more pronounced toward equatorial regions, such as where the earthquake in this study occurred. This latitudinal sensitivity of ionospheric responses to seismic events is explained by the findings of Zettergen and Snively (2015, 2019) and Occhipinti et al. (2008), indicating a greater sensitivity in low-latitude to equatorial regions compared to higher latitudes. Thus, the occurrence of this deep-focus earthquake at the equatorial region (see Figure 1) may have facilitated the detectability of the ionoquakes as well.

Lastly, Dautermann et al. (2009) noted that the efficiency of lithosphere-atmosphere-ionosphere coupling can vary with local time. Maruyama et al. (2012) observed that ionospheric signatures linked to earthquakes, characterized by multiple cusps in ionograms, are more prominently visible during local daytime. Therefore, the earthquake occurring at 16:00 local time was probably conducive to generating TEC disturbances associated with this event. However, future studies could explore these factors in greater detail, particularly focusing on modeling the lithosphere-atmosphere-ionosphere coupling under various seismic and ionospheric conditions to improve understanding and predictive capabilities in ionospheric seismology.

5 Summary and Conclusion

In conclusion, this study investigated the occurrence and characteristics of ionoquakes following a deep-focus earthquake near Tarauacá, Brazil, on 20th January 2024. The earthquake, with a magnitude of 6.6 and a focal depth of 607 km, exhibited minimal surface impact but generated detectable ionospheric disturbances. In this paper, we report the first coseismic ionospheric disturbances following the deep-focus 6.6 magnitude earthquake in the Brazilian sector. We performed a joint study of both the ground uplift which is obtained from the vertical component of the ground vibrations and the TEC disturbances in the ionosphere obtained from RBMC GNSS receivers (Rede Brasileira de Monitoramento Contínuo dos Sistemas GNSS | IBGE). The results show clear ground uplift and associated TEC disturbances with apparent "*N*-type" wave following the earthquake. From the properties of these ionoquakes such as the start time, propagating speed, and the dynamic spectrum we can infer that they were induced by the infrasonic-acoustic waves which were released from the

https://doi.org/10.5194/angeo-2024-16
Preprint. Discussion started: 19 September 2024

uplift/crustal displacement or a mixture of acoustic and gravity waves. The fact that the propagating speed of the ionoquakes fall between 550 m/s – 743 m/s which is within the thermospheric sound speed range (see Figure S1) and also the TEC disturbances peaking at the frequency 14 mHz - 16 mHz suggest the major role of infrasonic-acoustic waves and not Rayleigh waves signatures (Yeh and Liu, 1974). In addition, the strong correlation (which is statistically significance) between the ground uplift dynamic spectrum and the ionoquakes dynamic spectrum further reiterates the clear vertical coupling between the solid-earth and the overlaying atmosphere (Lognonne, 2006), the existence of energy flow from the lithosphere to the ionosphere (Kherani et al., 2009) and the potency of ionosphere serving as natural sensor of natural hazards (Astafyveva et al., 2019; Kherani et al., 2012). Understanding ionoquakes is crucial not only for advancing ionospheric seismology but also for enhancing our ability to monitor and predict ionospheric responses to seismic events, contributing to broader applications in geophysics and space weather research.

6 Competing interests

The contact author has declared that none of the authors has any competing interests.

7 Acknowledgements

We acknowledge our data sources such as the Brazilian Network for Continuous Monitoring of GNSS Systems (IBGE) for the TEC data, and United States Geological Survey (USGS) for the seismometers data. Oluwasegun Micheal Adebayo acknowledges the Brazilian National Council for Scientific and Technological Development (CNPq) for the PhD Fellowship (161901/2022-0). Esfhan Alam Kherani acknowledges support from FAPESP 2022/03502-6 and CNPq 307496/2015-5.

https://doi.org/10.5194/angeo-2024-16
Preprint. Discussion started: 19 September 2024

8 Open Research

The seismometer data used for this research can be obtained from the IRIS website and the TEC data can be obtained from the Rede Brasileira de Monitoramento Contínuo dos Sistemas GNSS | IBGE.

References

Afraimovich, E. L., Perevalova, N. P., Plotnikov, A. V., and Uralov, A. M.: The shock-acoustic waves generated by earthquakes, In *Annales Geophysicae,* Vol. 19, No. 4, pp. 395-409, https://doi.org/10.5194/angeo-19-395-2001, 2001.

Artru, J., Lognonné, P., and Blanc, E.: Normal modes modelling of post-seismic ionospheric oscillations, *Geophysical Research Letters*, *28*(4), 697-700, https://doi.org/10.1029/2000GL000085, 2001.

Astafyeva, E.: Ionospheric detection of natural hazards, *Reviews of Geophysics*, *57*(4), 1265-128, https://doi.org/10.1029/2019RG000668, 2019.

Astafyeva, E., and Heki, K.: Dependence of waveform of near-field coseismic ionospheric disturbances on focal mechanisms. *Earth, Planets and Space*, *61*, 939-943, https://doi.org/10.1186/BF03353206, 2009.

Astafyeva, E., and Shults, K.: Ionospheric GNSS imagery of seismic source: Possibilities, difficulties, and challenges, *Journal of Geophysical Research: Space Physics*, *124*(1), 534-543, https://doi.org/10.1029/2018JA026107, 2019.

Astafyeva, E., Rolland, L., Lognonné, P., Khelfi, K., and Yahagi, T.: Parameters of seismic source as deduced from 1 Hz ionospheric GPS data: Case study of the 2011 Tohoku-oki event, *Journal of Geophysical Research: Space Physics*, *118*(9), 5942-5950, https://doi.org/10.1002/jgra.50556, 2013.

Banks, P. M., and Kockarts, G.: *Aeronomy*. Elsevier, 2013.

Cahill, T., and Isacks, B. L.: Seismicity and shape of the subducted Nazca plate, *Journal of Geophysical Research: Solid Earth*, *97*(B12), 17503-17529, https://doi.org/10.1029/92JB00493, 1992.

https://doi.org/10.5194/angeo-2024-16
Preprint. Discussion started: 19 September 2024

Cahyadi, M. N., and Heki, K.: Coseismic ionospheric disturbance of the large strike-slip earthquakes in North Sumatra in 2012: M w dependence of the disturbance amplitudes, *Geophysical journal international*, *200*(1), 116-129, https://doi.org/10.1093/gji/ggu343 , 2015.

Castaños, H., and Lomnitz, C.: *Earthquake disasters in Latin America: A holistic approach,* Springer Science and Business Media, 2012.

Chum, J., Liu, J. Y., Laštovička, J., Fišer, J., Mošna, Z., Baše, J., and Sun, Y. Y. (2016). Ionospheric signatures of the April 25, 2015 Nepal earthquake and the relative role of compression and advection for Doppler sounding of infrasound in the ionosphere. *Earth, Planets and Space*, *68*, 1-12, https://doi.org/10.1186/s40623-016-0401-9 , 2016.

Dautermann, T., Calais, E., Lognonné, P., and Mattioli, G. S.: Lithosphere—atmosphere—ionosphere coupling after the 2003 explosive eruption of the Soufriere Hills Volcano, Montserrat, *Geophysical Journal International*, *179*(3), 1537-1546, https://doi.org/10.1111/j.1365-246X.2009.04390.x, 2009.

Davies, K., and Baker, D. M.: Ionospheric effects observed around the time of the Alaskan earthquake of March 28, 1964, *Journal of Geophysical Research*, *70*(9), 2251-2253, https://doi.org/10.1029/JZ070i009p02251, 1965.

De Santis, A., Marchetti, D., Spogli, L., Cianchini, G., Pavón-Carrasco, F. J., Franceschi, G. D., ... and Drimaco, D.: Magnetic field and electron density data analysis from swarm satellites searching for ionospheric effects by great earthquakes: 12 case studies from 2014 to 2016, *Atmosphere*, *10*(7), 371, https://doi.org/10.3390/atmos10070371, 2019.

Garcia, R. F., Klotz, A., Hertzog, A., Martin, R., Gérier, S., Kassarian, E., ... and Mimoun, D.: Infrasound from large earthquakes recorded on a network of balloons in the stratosphere, *Geophysical Research Letters*, *49*(15), https://doi.org/10.1029/2022GL098844, 2022.

Gonzalez, W. D., Joselyn, J. A., Kamide, Y., Kroehl, H. W., Rostoker, G., Tsurutani, B. T., and Vasyliunas, V. M.: What is a geomagnetic storm?, *Journal of Geophysical Research: Space Physics*, *99*(A4), 5771-5792, https://doi.org/10.1029/93JA02867 , 1994.

Hamama, I., and Yamamoto, M. Y.: Infrasonic earthquake detectability investigated in southern part of Japan, 2019. *Sensors*, *21*(3), 894, https://doi.org/10.3390/s21030894 , 2021.

https://doi.org/10.5194/angeo-2024-16
Preprint. Discussion started: 19 September 2024

Hasegawa, A., and Sacks, I. S.: Subduction of the Nazca plate beneath Peru as determined from seismic observations, *Journal of Geophysical Research: Solid Earth*, *86*(B6), 4971-4980, https://doi.org/10.1029/JB086iB06p04971 , 1981.

Heki, K.: Ionospheric disturbances related to earthquakes, *Geophysical Monograph 260, First Edition*, 511-526, DOI: 10.1002/9781119815617.ch21 , 2021.

Heki, K., Otsuka, Y., Choosakul, N., Hemmakorn, N., Komolmis, T., and Maruyama, T.: Detection of ruptures of Andaman fault segments in the 2004 great Sumatra earthquake with coseismic ionospheric disturbances, *Journal of Geophysical Research: Solid Earth*, *111*(B9), https://doi.org/10.1029/2005JB004202 , 2006.

Hines, C. O.: Internal atmospheric gravity waves at ionospheric heights, *Canadian Journal of Physics*, *38*(11), 1441-1481, https://doi.org/10.1139/p60-150 , 1960.

Hofmann-Wellenhof, B., Lichtenegger, H., and Wasle, E.: *GNSS–global navigation satellite systems: GPS, GLONASS, Galileo, and more,* Springer Science and Business Media, 2007.

Kelley, M. C.: *The Earth's ionosphere: Plasma physics and electrodynamics,* Academic press, 2009.

Kherani, E. A., Lognonne, P., Hébert, H., Rolland, L., Astafyeva, E., Occhipinti, G., ... and De Paula, E. R.: Modelling of the total electronic content and magnetic field anomalies generated by the 2011 Tohoku-Oki tsunami and associated acoustic-gravity waves, *Geophysical Journal International*, *191*(3), 1049-1066, https://doi.org/10.1111/j.1365-246X.2012.05617.x , 2012.

Kherani, E. A., Rolland, L., Lognonné, P. H., Sladen, A., Klausner, V., and de Paula, E. R.: Traveling ionospheric disturbances propagating ahead of the Tohoku-Oki tsunami: a case study, *Geophysical Journal International*, *204*(2), 1148-1158, doi: 10.1093/gji/ggv500, 2016.

Krischer, L., Megies, T., Barsch, R., Beyreuther, M., Lecocq, T., Caudron, C., and Wassermann, J.: ObsPy: A bridge for seismology into the scientific Python ecosystem, *Computational Science and Discovery*, *8*(1), 014003, DOI 10.1088/1749-4699/8/1/014003, 2015.

Li, L., Jin, S., and Chai, Y.: Co-seismic ionospheric disturbances characteristics in different azimuths following the 2022 Mexico earthquake from GNSS observations. *GPS Solutions*, *28*(1), 23, https://doi.org/10.1007/s10291-023-01564-9 , 2024.

https://doi.org/10.5194/angeo-2024-16
Preprint. Discussion started: 19 September 2024

Lognonné, P., Artru, J., Garcia, R., Crespon, F., Ducic, V., Jeansou, E., ... and Godet, P. E.: Ground-based GPS imaging of ionospheric post-seismic signal, *Planetary and Space Science*, *54*(5), 528-540, https://doi.org/10.1016/j.pss.2005.10.021 , 2006.

Lognonné, P., Clévédé, E., and Kanamori, H.: Computation of seismograms and atmospheric oscillations by normal-mode summation for a spherical earth model with realistic atmosphere, *Geophysical Journal International*, *135*(2), 388-406, https://doi.org/10.1046/j.1365-246X.1998.00665.x , 1998.

Lognonné, P., Garcia, R., Crespon, F., Occhipinti, G., Kherani, A., and Artru-Lambin, J.: Seismic waves in the ionosphere, *Europhysics News*, *37*(4), 11-15, 2006.

Maletckii, B., Astafyeva, E., Sanchez, S. A., Kherani, E. A., and De Paula, E. R.: The 6 February 2023 Türkiye earthquake sequence as detected in the ionosphere, *Journal of Geophysical Research: Space Physics*, *128*(9), https://doi.org/10.1029/2023JA031663 , 2023.

Maruyama, T., Tsugawa, T., Kato, H., Ishii, M., and Nishioka, M.: Rayleigh wave signature in ionograms induced by strong earthquakes, *Journal of Geophysical Research: Space Physics*, *117*(A8), https://doi.org/10.1029/2012JA017952 , 2012.

Molchanov, O. A., Hayakawa, M., and Rafalsky, V. A.: Penetration characteristics of electromagnetic emissions from an underground seismic source into the atmosphere, ionosphere, and magnetosphere, *Journal of Geophysical Research: Space Physics*, *100*(A2), 1691-1712, https://doi.org/10.1029/94JA02524 , 1995.

Occhipinti, G., Kherani, E. A., and Lognonné, P.: Geomagnetic dependence of ionospheric disturbances induced by tsunamigenic internal gravity waves, *Geophysical Journal International*, *173*(3), 753-765, https://doi.org/10.1111/j.1365-246X.2008.03760.x , 2008.

Parrot, M., and Mogilevsky, M. M.: VLF emissions associated with earthquakes and observed in the ionosphere and the magnetosphere, *Physics of the Earth and Planetary Interiors*, *57*(1-2), 86-99, https://doi.org/10.1016/0031-9201(89)90218-5 , 1989.

Perevalova, N. P., Sankov, V. A., Astafyeva, E. I., and Zhupityaeva, A. S.: Threshold magnitude for ionospheric TEC response to earthquakes, *Journal of Atmospheric and Solar-Terrestrial Physics*, *108*, 77-90, https://doi.org/10.1016/j.jastp.2013.12.014 , 2014.

https://doi.org/10.5194/angeo-2024-16
Preprint. Discussion started: 19 September 2024

Rolland, L. M., Lognonné, P., Astafyeva, E., Kherani, E. A., Kobayashi, N., Mann, M., and Munekane, H.: The resonant response of the ionosphere imaged after the 2011 off the Pacific coast of Tohoku Earthquake, *Earth, planets and space*, *63*, 853-857, https://doi.org/10.5047/eps.2011.06.020 , 2011.

Rolland, L. M., Vergnolle, M., Nocquet, J. M., Sladen, A., Dessa, J. X., Tavakoli, F., ... and Cappa, F.: Discriminating the tectonic and non-tectonic contributions in the ionospheric signature of the 2011, Mw7. 1, dip-slip Van earthquake, Eastern Turkey, *Geophysical Research Letters*, *40*(11), 2518-2522, doi:10.1002/grl.50544, 2013, 2013.

Ruan, Q., Yuan, X., Liu, H., and Ge, S.: Study on co-seismic ionospheric disturbance of Alaska earthquake on July 29, 2021 based on GPS TEC. *Scientific Reports*, *13*(1), 10679, https://doi.org/10.1038/s41598-023-37374-9 , 2023.

Sanchez, S. A., Kherani, E. A., Astafyeva, E., and De Paula, E. R.: Rapid Detection of Co-Seismic Ionospheric Disturbances Associated With the 2015 Illapel, the 2014 Iquique and the 2011 Sanriku-Oki Earthquakes, *Journal of Geophysical Research: Space Physics*, *128*(9), https://doi.org/10.1029/2022JA031231 , 2023.

Sanchez, S. A., Kherani, E. A., Astafyeva, E., and de Paula, E. R.: Ionospheric disturbances observed following the ridgecrest earthquake of 4 July 2019 in California, USA, *Remote Sensing*, *14*(1), 188, https://doi.org/10.3390/rs14010188 , 2022.

Sharma, D. K., Israil, M., Chand, R., Rai, J., Subrahmanyam, P., and Garg, S. C.: Signature of seismic activities in the F2 region ionospheric electron temperature, *Journal of atmospheric and solar-terrestrial physics*, *68*(6), 691-696, https://doi.org/10.1016/j.jastp.2006.01.005 , 2006.

Sunil, A. S., Bagiya, M. S., Bletery, Q., and Ramesh, D. S.: Association of ionospheric signatures to various tectonic parameters during moderate to large magnitude earthquakes: Case study. *Journal of Geophysical Research: Space Physics*, *126*(3), https://doi.org/10.1029/2020JA028709 , 2021.

Sunil, A. S., Bagiya, M. S., Catherine, J., Rolland, L., Sharma, N., Sunil, P. S., and Ramesh, D. S.: Dependence of near field co-seismic ionospheric perturbations on surface deformations: A case study based on the April, 25 2015 Gorkha Nepal earthquake, *Advances in Space Research*, *59*(5), 1200-1208, DOI: 10.1016/j.asr.2016.11.041, 2017.

https://doi.org/10.5194/angeo-2024-16
Preprint. Discussion started: 19 September 2024

Sunil, A. S., Sunil, P. S., Shrivastava, M. N., Maurya, A. K., Thomas, D., and Gonzalez, G.: Seismic induced ground deformation and ionospheric perturbations of the 29 July 2021, Mw 8.2 Chignik Earthquake, Alaska. *Journal of Geophysical Research: Space Physics*, *127*(11), e2022JA030576, https://doi.org/10.1029/2022JA030576 , 2022.

Takeya, M. K. (1992). High precision studies of an intraplate earthquake sequence in northeast Brazil.

Tanaka, T., Ichinose, T., Okuzawa, T., Shibata, T., Sato, Y., Nagasawa, C., and Ogawa, T.: HF-Doppler observations of acoustic waves excited by the Urakawa-Oki earthquake on 21 March 1982. *Journal of atmospheric and terrestrial physics*, *46*(3), 233-245, https://doi.org/10.1016/0021-9169(84)90150-8 , 1984.

Torrence, C., and Compo, G. P.: A practical guide to wavelet analysis. *Bulletin of the American Meteorological society*, *79*(1), 61-78, https://doi.org/10.1175/1520-0477(1998)079<0061:APGTWA>2.0.CO;2 , 1998.

Vashisth, S., Gera, S. K., Ammani, A., Singh, P., Pandey, P., Kumari, S., and Mishra, O. P. (2024). Co-seismic ionospheric disturbances due to 2004 Sumatra-Andaman earthquake. *Quaternary Science Advances*, *13*, 100148, https://doi.org/10.1016/j.qsa.2023.100148 , 2024.

Virtanen, P., Gommers, R., Oliphant, T. E., Haberland, M., Reddy, T., Cournapeau, D., ... and Van Mulbregt, P.: SciPy 1.0: fundamental algorithms for scientific computing in Python, *Nature methods*, *17*(3), 261-272, https://doi.org/10.1038/s41592-019-0686-2 , 2020.

Yeh, K. C., and Liu, C. H.: Acoustic-gravity waves in the upper atmosphere. *Reviews of Geophysics*, *12*(2), 193-216, https://doi.org/10.1029/RG012i002p00193 , 1974.

Zettergren, M. D., and Snively, J. B.: Ionospheric response to infrasonic-acoustic waves generated by natural hazard events, *Journal of Geophysical Research: Space Physics*, *120*(9), 8002-8024, https://doi.org/10.1002/2015JA021116 , 2015.

Zettergren, M. D., and Snively, J. B.: Latitude and longitude dependence of ionospheric TEC and magnetic perturbations from infrasonic-acoustic waves generated by strong seismic events, *Geophysical Research Letters*, *46*(3), 1132-1140, https://doi.org/10.1029/2018GL081569 , 2019.

https://doi.org/10.5194/angeo-2024-16
Preprint. Discussion started: 19 September 2024


Annales Geophysicae Discussions

Zhai, C., Yao, Y., and Kong, J.: Three-dimensional reconstruction of seismo-traveling ionospheric disturbances after March 11, 2011, Japan Tohoku earthquake. *Journal of Geodesy*, *95*(7), 77, DOI: 10.1007/s00190-021-01533-5, 2021.

Zhang, X., Shen, X., Liu, J., Ouyang, X., Qian, J., and Zhao, S.: Analysis of ionospheric plasma perturbations before Wenchuan earthquake, *Natural Hazards and Earth System Sciences*, *9*(4), 1259-1266, https://doi.org/10.5194/nhess-9-1259-2009, 2009.